LIVE L4 AND LIVE L5L EXPERIMENTS ON MELT POOL AND CRUST BEHAVIOUR IN THE RPV LOWER HEAD

X. Gaus-Liu¹, A. Miassoedov¹, J. Foit¹, T. Cron¹, F. Kretzschmar, T. Wenz¹, S. Schmidt-Stiefel¹

¹ Karlsruhe Institute of Technology, Eggenstein-Leopoldshafen, Germany xiaoyang.gaus-liu@kit.edu, alexei.miassoedov@kit.edu, jerzy.foit@kit.edu, thomas.cron@kit.edu, frank.kretzschmar@kit.edu, thomas.wenz@kit.edu, silke.schmidt-stiefel@kit.edu

Abstract

LIVE-L4 and LIVE-L5L experiments investigated thermal hydraulic behavior of corium pool in the RPV lower head with a 3D test vessel LIVE. The simulant material is 80%-20% KNO₃-NaNO₃. Transient and steady-state parameters such as melt temperature, heat flux distribution through the vessel wall as well as crust formation characteristics were obtained. The two tests demonstrated that transient events like melt relocation and change of decay power facilitate crust deformation and change of crust thickness. The dimensionless melt temperature and heat flux through wall during the steady state can be well described independent of power density. However the dimensionless melt temperature and heat flux are dependent on the pool height. A low pool has stronger focusing effect at the upper surface than in a high pool.

1. Introduction

The behaviour of the corium pool in the RPV lower head is still a critical issue in the understanding of Pressurized Water Reactors (PWR) core meltdown accidents. The current concerns related with the understanding of in-vessel core melting severe accident include its course, critical phases and timing, and their influence on the accident progression. There are still open questions related to the steady-state thermal hydraulic behaviour of a melt pool although it has been extensively studied. Additionally, many uncertainties exist in the description of the transient melt behaviour, such as characteristics of corium arrival in the lower head, and change of power density in the corium pool due to debris melting and melt relocation. These phenomena are plant and accident sequence dependent and can have strong impacts on the potential termination of a severe accident [5], [6].

It is necessary to study the transient and steady state core melt phenomena as a whole process to provide a reasonable estimation of the remaining uncertainty band in regard to safety assessment. It is also of great interest to identify the distribution of melt temperature and heat flux in a three-dimensional hemispherical geometry, so that their data can be compared with the ones obtained from slice test facilities or cylinder test vessel [3], [4]. To complement the experimental data on in–vessel melt pool behaviour, Karlsruhe Institute of Technology (KIT) performs large-scale tests in the LIVE program, which investigates the core melt behaviour in the lower plenum of the reactor pressure vessel and the effect of external water cooling under conditions that may occur during core meltdown accident in PWRs [7]-[10]. The information from LIVE experiments is being used for the validation and implementation of severe accident codes like CONV and ASTEC [11]-[13].

2. Test description

The hemispherical test vessel of LIVE has a diameter of 1 m. The main components in the test vessel are shown in Figure 1. The top area of the test vessel can be either insulated with a lid or be cooled with a water container. The test vessel is enclosed in a cooling vessel to enable external water cooling. The decay heat of the melt is simulated by 6 planes of heating coils, which can be controlled individually to simulate homogenous heat generation. The melt is prepared in a separated heating furnace and can be released to the test vessel either centrally or near the vessel wall. A vacuum pump extracts the residual melt back to the heating furnace at the end of test.

The test vessel has extensive instrumentation [14].Melt pool temperature was measured both with 36 thermocouples distributed in even distance in the melt and with a precise crust detection probe, which measures melt boundary temperature and melt temperature profile. vertical temperatures of the wall inner and outer surface were measured at 5 latitudes and 4 locations at each latitude. Heat flux distribution through the vessel wall can be obtained based these temperatures. Crust on solidification process was monitored with thermocouple trees intruding from the wall inner surface to the melt

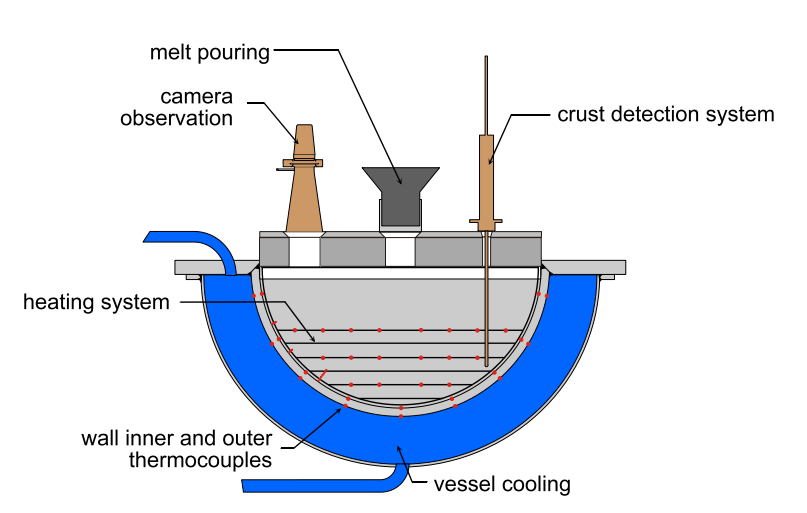


Figure 1 LIVE test facility with insulation lid

at three locations. Two video cameras and one infrared camera were used to visualise the convection of the melt pool.

The information obtained from the LIVE experiments includes the transient and steady-state melt temperature and heat flux distribution; motion of melt surface flow; crust growth velocity and crust thermal conductivity. In post-test analysis the bulk melt liquidus temperature, crust thickness profiles, crust composition and crust morphology were determined.

The test conditions in L4 and L5L were simular. In both tests the test vessel was insulated at the top and externally cooled with water under almost isothermal condition. Non-eutectic binary material KNO₃-NaNO₃ in 80%-20% mole relation was used as simulant material of corium [15]. The solidus temperature is about 220°C and the liquidus temperature is about 284°C [16]-[17]. The melt with 430 mm height was heated homogenously from bottom to 310 mm. In both tests there were heating periods in time order of 18 kW, 10 kW, 5 kW and 10 kW. 18 kW is the possible maximum homogenous heat dissipation rate for the test. The repetition of 10 kW and 18 kW was aimed to examine the effect of crust formation and remelting on the melt pool parameters. The main difference between the two tests was the number of melt releases. The melt of 210 l in total was poured in two charges in LIVE-L5L: 120 l in the first charge and 90 l in the second charge; whereas only one melt pouring was performed in L4.

3. Test results

3.1 Transient behaviour of melt pool

3.1.1 <u>Transient melt pool temperature</u>

The melt with originally 342 °C was poured into the test vessel at room temperature within 100 seconds and was cooled to 330 °C when the pouring process was finished. Then the melt pool underwent a temperature stratification process, in which the lower part of the melt cooled down further whereas the melt temperature in the pool upper layer increased firstly and then reduced to a steady value. It took about 2000 seconds for the whole pool to reach steady temperatures. The transient melt temperatures after melt releases and power reductions in L5L test are shown in Figure 2. After heating power reduction, the melt temperature in the upper region decreased more slowly than in the pool lower part.

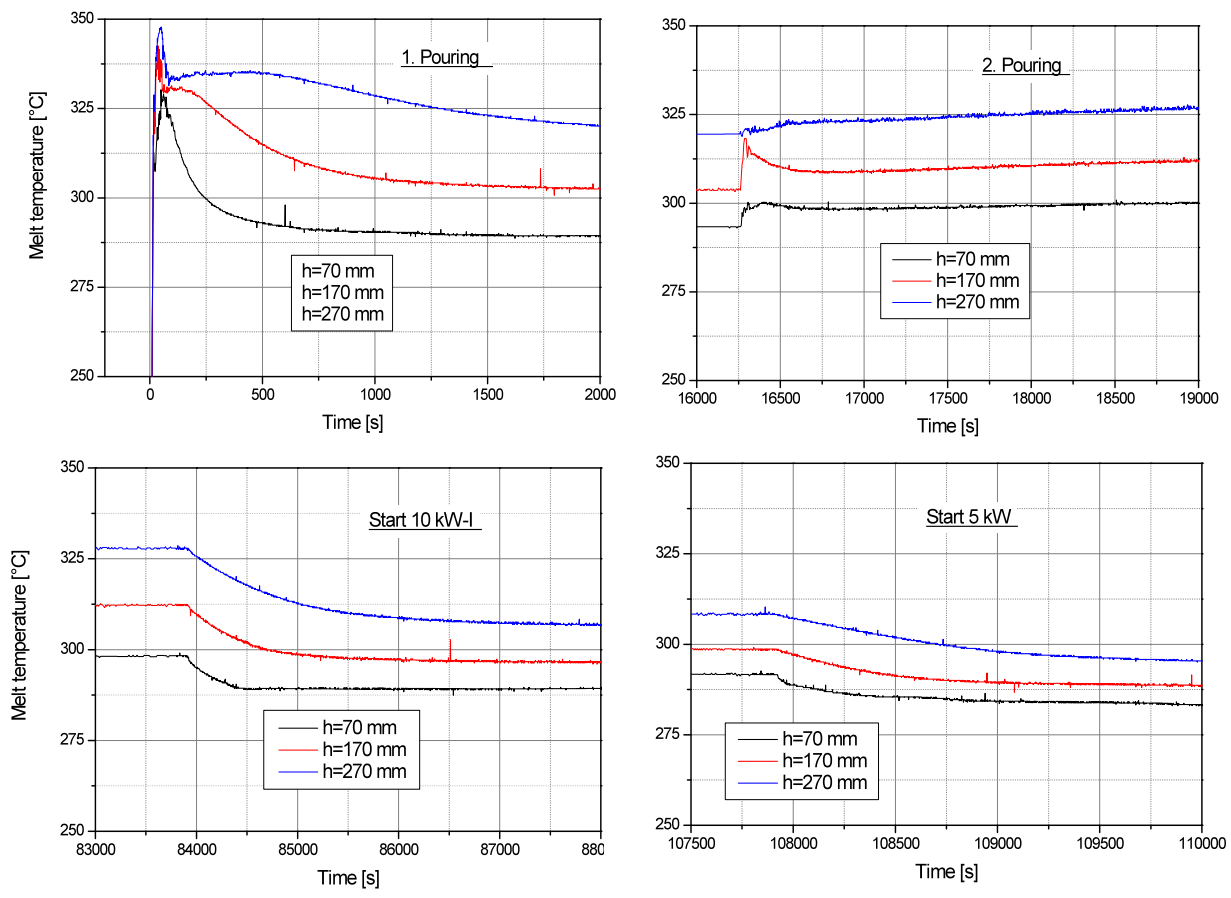
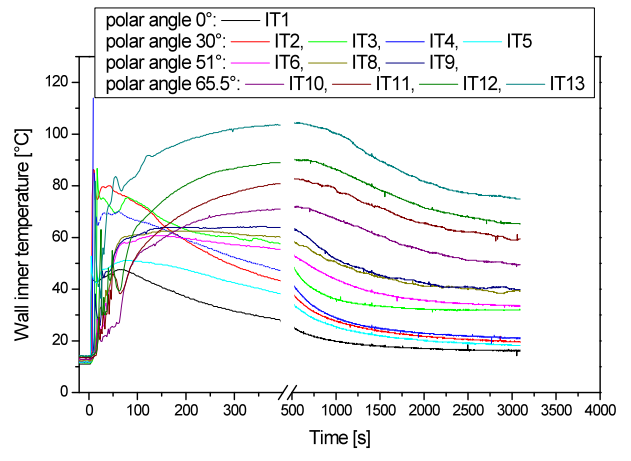


Figure 2 Transient melt temperature after melt pouring and heating power reduction in LIVE L5L test

3.1.2 Transient heat flux

Depending on the position, the transient wall inner surface temperature and the transient heat flux reached their maximum values during or shortly after the melt pouring process. At the lower part of the vessel wall the peak values only lasted several seconds during the melt pouring

period, whereas at the wall upper area the peak values occurred at about 500 s after the initiation of melt pouring and reduced gradually to a steady value. Figure 3 shows the wall inner temperature and Figure 4 shows the heat flux from the beginning of melt pouring.



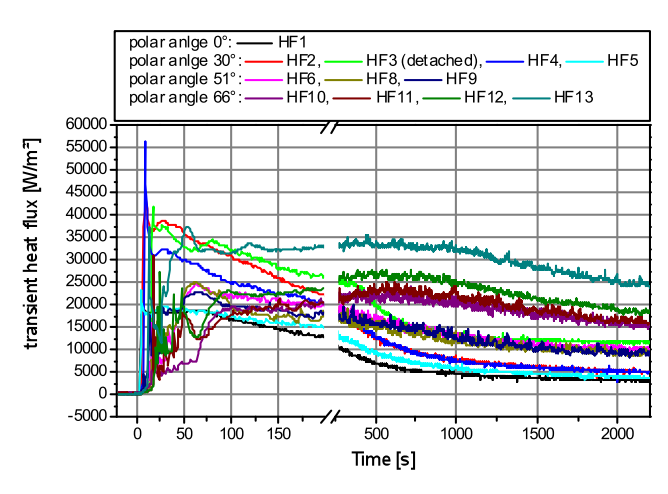


Figure 3 Wall inner temperatures after the first melt pouring in L5Ltest

Figure 4 Transient heat flux through vessel wall after the first melt pouring in L5L test

3.1.3 <u>Influence of melt pouring times and power density variation</u>

Melt relocation from the core region to the lower head in the reactor vessel can occur more than once during the core melting accident. It is found that repeated melt relocation and the variation

of power density exert strong thermo-mechanical stress on the crust layer at the vessel wall due to the density difference between solid and liquid melt [16], [18], [20]. To reduce or to release the stress, the crust layer reacts with gap formation at the crust/wall interface and/or building up cracks. Such events can occur repeatedly und their exact timing is unpredictable. The consequences of gap formation and crack building are different. The gap between crust and vessel wall acts as good insulation and results in melting of crust. In contrary, the crack through the crust layer enables the penetration of hot melt through the crust to the gap, there the hot melt solidifies and reduces the heat resistance from crust to the wall. As result the crust grows thicker to compensate the total heat resistance. Figure 5 shows a crust with a separable layer adjacent to the wall,



Figure 4 crust with easily separated layer at the wall in L5L test test

which is an evidence of the later solidified melt in the gap. A thicker crust must endure stronger stress than a thinner one, thus crust cracking is expected to occur more often in thicker crust. Figure 5 shows the events of gap formation and crust cracking at polar angle 52.9° during L5L test. The promt increase of crust temperature at the crust/wall interface, which was measured by thermocouple CT21, implies the poor cooling condition of the crust after a gap formation at the crust/wall interface. During the 5 kW heating period, the crust temperature decreased suddenly,

indicating an improved cooling at the crust/wall interface. The improved cooling is resulted by filling the gap with hot melt, which penetrated through the crust to the wall.

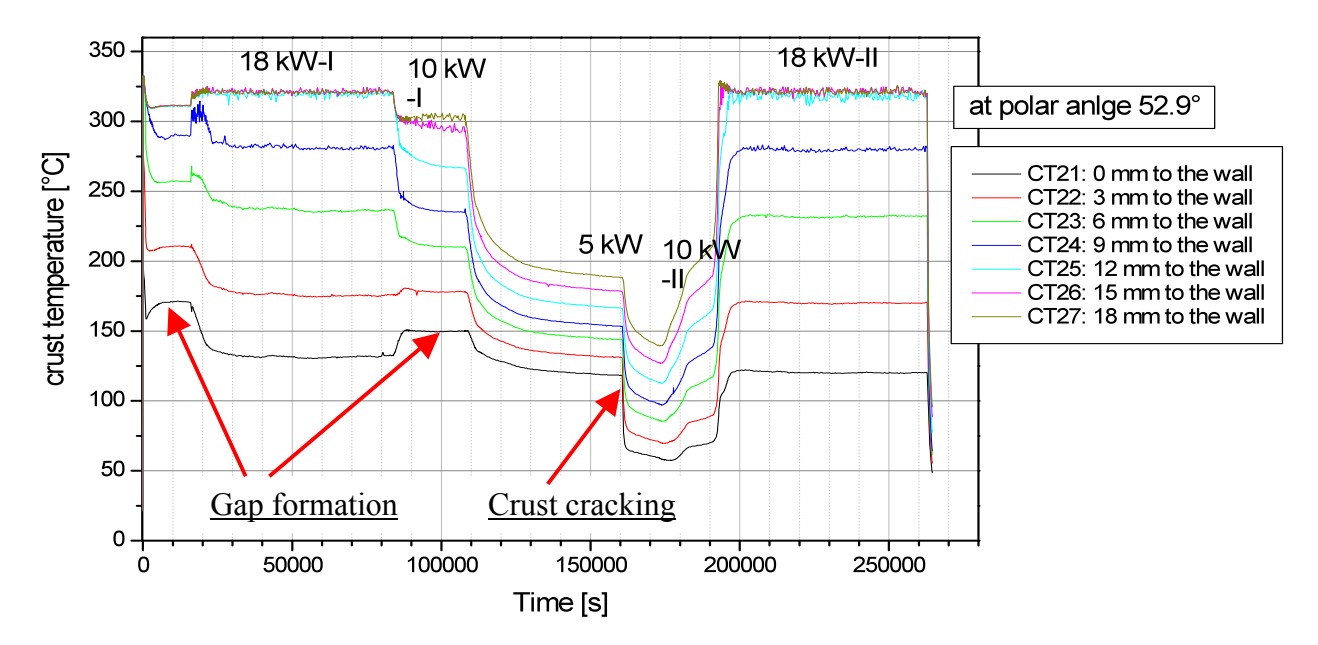


Figure 5 Crust temperature at polar angle 52.9° in L5L test with the implications of gap formation and hot melt penetration after crust cracking.

3.2 Steady-state behaviour of melt pool

3.2.1 Steady state melt temperature

a) Horizontal temperature distribution:

The melt temperatures at the upper layer of melt pool during 18 kW and 10 kW are relatively homogenous. The homogeneity improves with the power density. At 270 mm height, the temperature difference was within 1° C at 18 kW and within 3 °C at 10 kW. At the lower part of the pool larger temperature differences were measured. At height 170 mm, the temperature difference was within 4 °C at 18 kW and within 6 °C at 10 kW. There was no trend of temperature decrease from the central area to the vessel wall except at the boundary area. At 5 kW the horizontal temperature difference lays within the measurement error range of ± 1.5 °C.

b) Vertical melt temperature distribution:

At the lower layer the melt temperatures were measured at vessel height 70 mm, 170 mm and 270 mm; at the upper layer the melt temperatures at radius 365 mm were measured with the crust detection lance. When the dimensionless melt temperature in term of local temperature difference between melt temperature and interface temperature, $(T-T_{int})/(T_{mean}-T_{int})$ or $\Delta T/\Delta T_{mean}$, is plotted versus the dimensionless height in term of height/vessel radius, Figure 6

shows the vertical temperature profiles at the lower layer and Figure 7 shows the ones at the upper layer in L5L test. Here, T_{mean} is the global mean temperature and T_{int} is the interface temperature, taken to be that of the liquidus temperature corresponding to the melt bulk composition. The global mean temperature is the sum of weighted local melt temperatures, which are weighted by their occupied melt volume fractions.

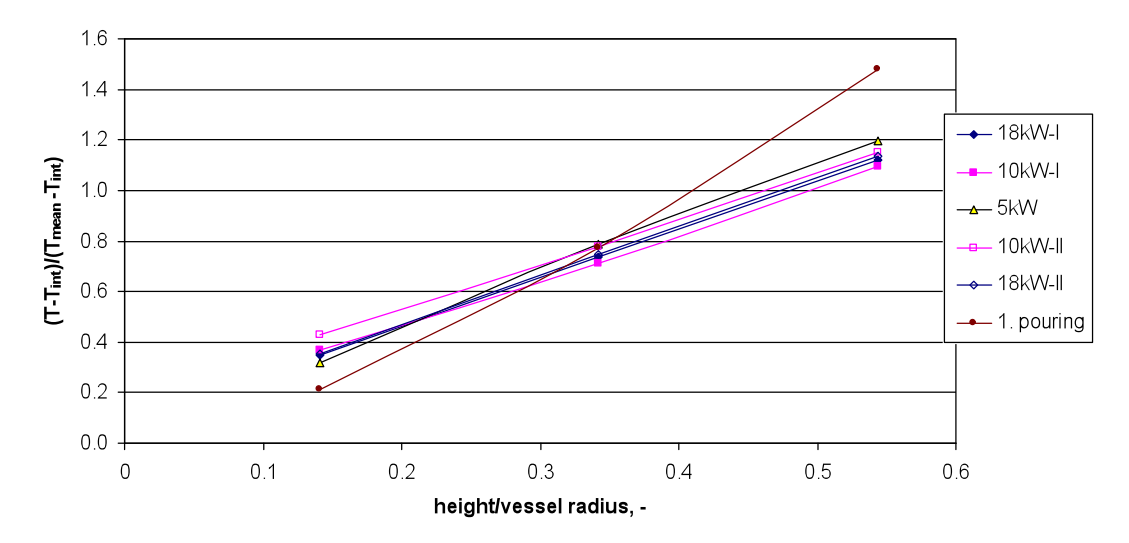


Figure 6 Demensionless melt temperature vertical profiles of the melt lower layer during the steady states of the heating periods in L5L test

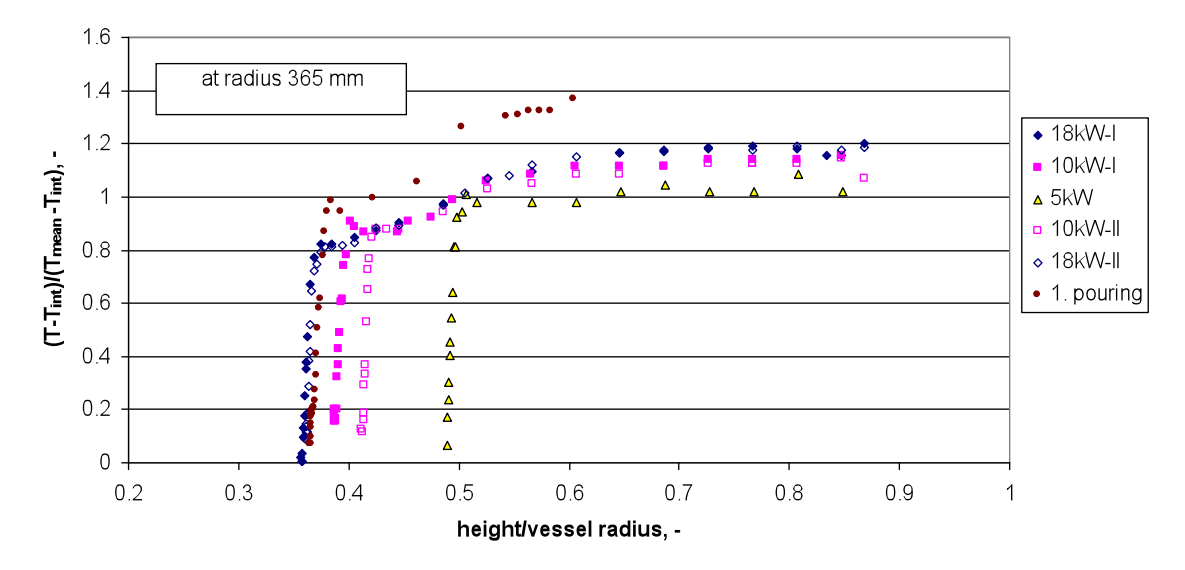


Figure 7 Dimensionless melt temperature difference (T-T_{int})/(T_{mean}-T_{int}) in L5L tests

Combining Figure 6 and Figure 7, three melt regions are identified: a) a 4-5 mm-thick boundary layer adjacent to the melt/crust interface, b) a temperature-stratified lower layer and c) a temperature-homogenous upper layer. Under the same melt height the dimensionless temperatures were identical independent of power density, e.g. after second melt pouring at 18 kW, 10 kW and 5 kW periods. The transition position between the stratified layer to the homogenous layer, which is in the term of the height ratio H_{tr}/H_{pool} , is about 0.7 for 430 mm

height pool. The temperature at the upper layer is about 1.2 times of the global mean temperature for a 430 mm-height pool.

Reducing the pool height to 300 mm, e.g. after the first melt pouring, results in a larger slop of dimensionless melt temperature at the stratified pool and a higher dimensionless temperature at the upper layer. Also the transition position of the two melt regimes moves upwards. Above results implies that the dimensionless melt temperature can be well described at same pool height, and it is a function of the pool height.

The dependency of ΔT_{mean} with the power density q in the pool can be analysed. For a melt pool in a hemispheric vessel with internal heat sources, ΔT_{mean} can be described in Eq(1). Eq (1) shows that the $\Delta T_{mean}/q$ is a function of pool height and Nu.

$$\Delta T_{mean} = \frac{\varphi}{h} = \frac{qH^2(3 - \frac{H}{R})}{6\lambda Nu} \tag{1}$$

Where:

φ is the average heat flux through vessel wall, [W/m²], which can be described as

$$\varphi = q \frac{Volume}{Surf\ ace} = q \frac{\frac{1}{3}\pi H^2(3R - H)}{2\pi RH} = \frac{1}{6}qH(3 - \frac{H}{R})$$
 (2)

h is the heat transfer coefficient, $[W/(m^2 \cdot K)]$,

$$h = \frac{\lambda N u}{H} \tag{3}$$

q: power density, [W/m³]

H: melt height, [m]

R: vessel radius, [m]

 λ : thermal conductivity of the melt, [W/(m·K)]

The temperature profiles within the boundary layer can be measured in detail by the crust detection lance, which is shown in Figure 8. The temperature gradients within the boundary layer are about 9 °C/mm, 6 °C/mm and 4 °C/mm at 18 kW, 10 kW and 5 kW respectively.

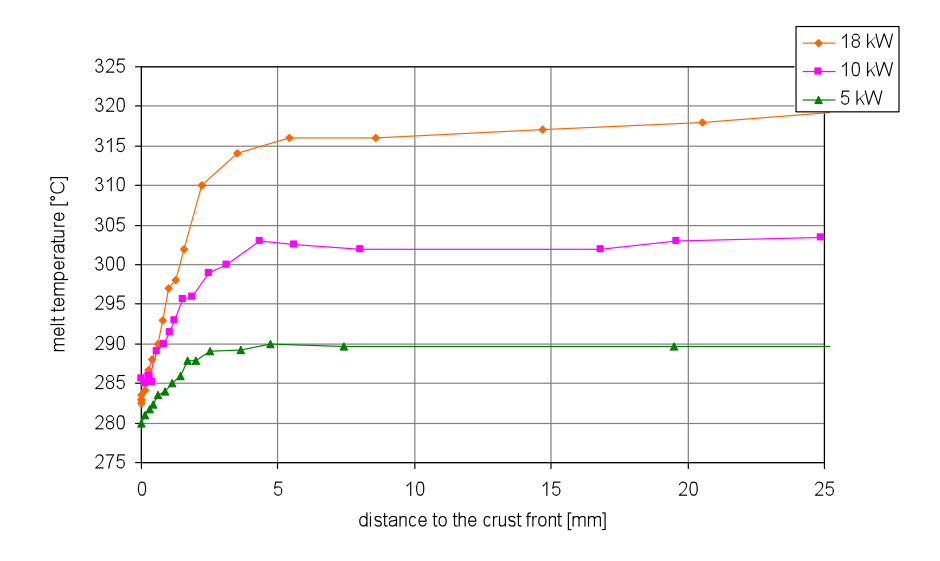


Figure 8 Melt temperature near the crust/melt interface at polar angle 47° measured with the crust detection lance

3.2.2 Steady state heat flux and heat balance

The heat flux through a local position of the vessel wall was calculated based on the difference between local wall inner surface temperature (IT) and outer surface temperature (OT) [14]. The system errors of IT-OT were corrected by calibrating the thermocouples in isothermal environment. The standard deviation of local heat flux was \pm 5% and the standard error was \pm 1%. The mean heat flux at a horizontal level, where several pairs of IT/OT located, was the mean value of the local heat fluxes. Some IT thermocouples were defected during the test, thus only the local heat fluxes calculated with intact IT thermocouples are considered. Relatively large deviations of horizontal mean values (\pm 10% to \pm 20%) are noticed. The real heat flux from the liquid melt to the crust should be horizontally uniform since the melt temperature is horizontally uniform and the interface temperature was the liquidus temperature of the actual melt composition. The uncertainty probably came from the uncertainty of IT thermocouples which are clamped in a slot at the wall inner surface. The measurement points in the thermocouples have more or less contact with the steel wall or with the environment next to the wall. The change of local environment at the crust/wall interface due to gap formation or crust cracking could affect the measurement results of the IT thermocouples.

Nevertheless the horizontal mean heat flux during different power densities are compared in their quantities (q) and normalized values weighted by the global mean heat flux (q/q_{mean}), as shown in Figure 9 and in Figure 10, respectively. The heat flux vertical distribution can be described as following: a) increasing power density only increases significantly the heat flux upon polar angle 30°; b) heat fluxes under same melt power density but during different heating periods were well comparable, such as the heat flux during 18 kW-I and 18 kW-II periods, and during 10 kW-I and 10 kW-II periods; c) The focusing effect of heat flux near melt surface (q_{max}/q_{mean}) in a small melt pool, e.g. the 120 l, was more significant ($q_{max}/q_{mean} = 2$) than the large melt pool in which the value was between 1.64 to 1.75. However, the absolute value of the maximum heat flux in a

large pool is higher than in a small pool. There is almost no heat flux focusing effect at the upper surface when the power density was very low.

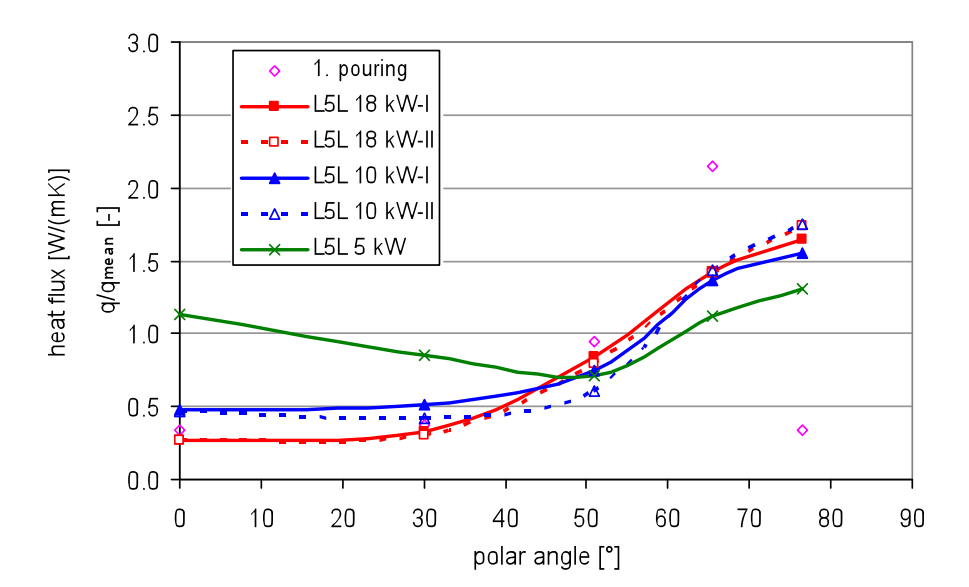


Figure 9 Distribution of steady state horizontal mean heat flux in L5L test

Figure 10 Distribution of weighted horizontal heat flux in terms of q/q_{mean} in L5L

Due to the lowest heating plane near the vessel bottom the heat flux at the vessel bottom was probably overestimated comparing absolutely homogenous volumetric heating. The overestimation was especially obvious at low heating power in which the crust growth over the lowest heating plane was significantly prohibited. The heat dissipation from the lowest heating plane resulted in a pit at the crust which can be still measured during 18 kW period, as shown in the crust thickness profiles in Figure 13.

The heat balance among the heat input Q_{heat} , the heat removed through vessel wall below the melt surface Q_{wall} , the heat removed from the external cooling water are determined. The data are given in Table 1. The ratio of $Q_{\text{wall}}/Q_{\text{heat}}$ decreased with lowering power density; however the ratios of $Q_{\text{water}}/Q_{\text{heat}}$ were comparable during various power densities. This implies that the heat loss have two sources: the heat loss through the openings of the insulation lids amounts 20% of all power density, and the rest is through the vessel sidewall above the melt surface. This fraction increases with the decreasing power density. Some important melt and heat transfer parameters are generalized in Table 1.

heating power, kW	1. pouring 10 kW.	2. pouring 18 kW-I	10 kW-II	5 kW	10 kW-II	18 kW-II
Melt T mean, °C	310.6	323.2	305.2	289.8	305.8	323.1
Melt T _{max} , °C	320.8	331.3	309	290.7	309	330.7
T _{int} , °C	283.2	282.8	281.2	279.2	280.7	283.4
Heating Q _{heating} , W	9959	18088	9967	4999	10013	18066
Q _{wall,} W	7667	14844	7554	2942	7345	13963
Qwall/Qheating, -	0.77	0.81	0.73	0.59	0.74	0.78
Qwater/Qheating	0.93	0.84 (9	$/14)^{0.85}$	0.84	0.84	0.84
Power density, W/m ³	84008	87970	48384	27267	48608	87701
Heat flux, q _{dn mean} , W/m ²	7960	10900	5514	2206	5504	10442

Table 1 Some steady-state melt and heat transfer parameters in L5L test

3.3 Crust formation characteristics and their influence on heat transfer

The crust growth process can be monitored with crust temperature thermocouple trees at polar angle 37.6°, 52.9° and 66.9° [10]. Figure 11 shows the crust thickness progression after the first melt pouring in L5L test. According to the criterion of constitutional supercooling condition of the nitrate simulate melt [19], the time period of the constitutional supercooling, in which mushy zone exists, was less than 4000 s at 52.9°, and 5000 s at 37.6°.

The crust thicknesses at the thermocouple tree positions during the test can be roughly estimated, as shown in Figure 12. The crust thickness differed considerably at some locations at the same power density but different heating periods. This phenomenon could be a result of local gap formation and crust cracking. The crust profiles at the end of the test were measured at four azimuth angles. Figure 13 shows the crust profiles at the end of 18 kW heating period in L5L test. The pits at the vessel bottom and some other locations in the lower part of the crust were caused by the local heating coils. A gap is observed between crust layer and the vessel wall after the test. The crust thicknesses including gap at the upper part of the vessel are comparable, whose deviation was less than 5 mm.

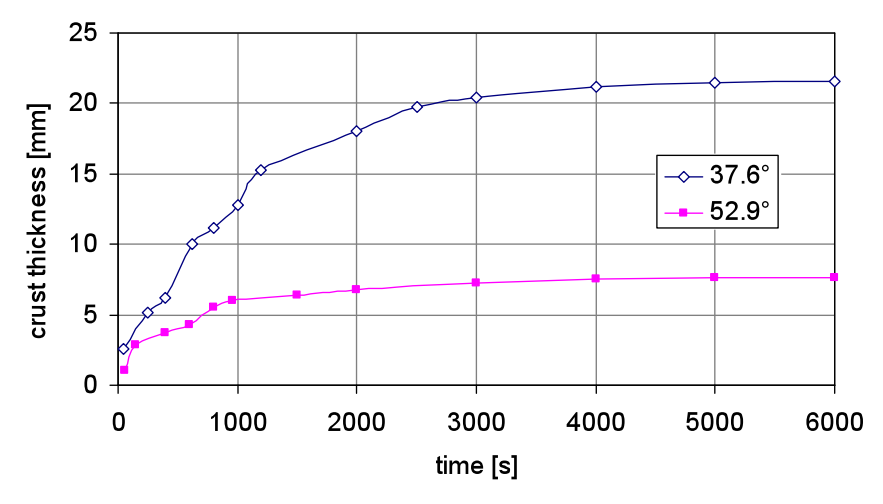


Figure 11 Crust thickness progression after the first melt pouring in L5L test

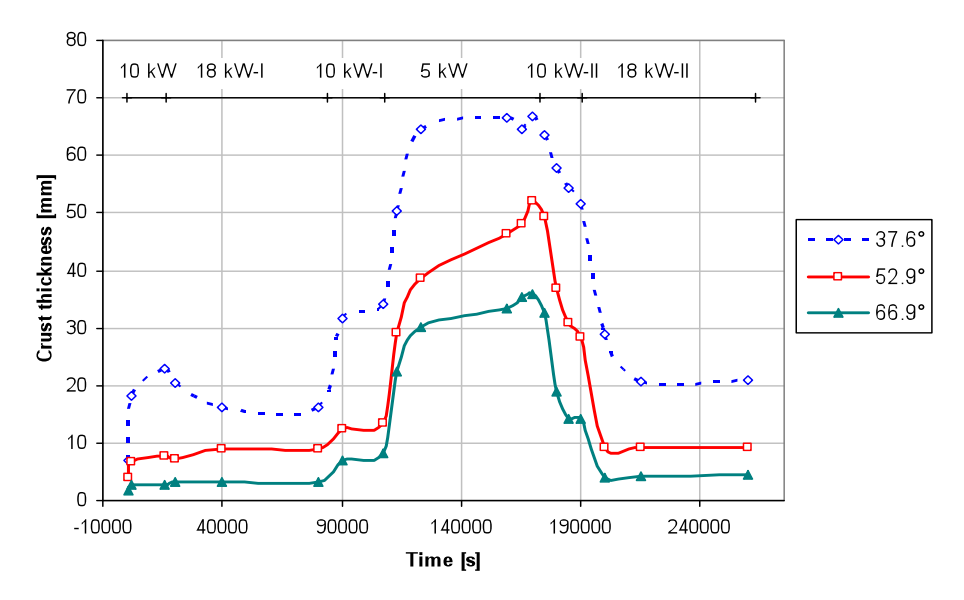


Figure 12 Crust thickness at polar angle 37.6°, 52.9° and 66.9° during the L5L test period

The crust thermal conductivity during different heating periods was calculated according to crust temperature and the horizontal mean heat flux through vessel wall. The accuracy of the crust thermal conductivity calculation was subjected to the deviation of the horizontal mean heat flux. The crust thermal conductivity at a local position in the crust cross section ranged from 0.4 to 0.8 W/(m·K), which also varied during different heating periods. The general thermal conductivity through a crust cross section lay between 0.43 and 0.7 W/(m·K).

The crust formation could exert significant influence on the heat transfer through the vessel sidewall by changing the melt/crust interface temperature. The interface temperature depends on the actual bulk melt composition, which becomes enriched in low-melting component of the melt during crust formation process, e.g. NaNO₃ in the 80% KNO₃ – 20% NaNO₃ mixture. Especially the heat transfer in the melt pool with low power density reacts intensively with the crust formation process, since the mean temperature difference, T_{mean} - T_{int} , can increase significantly comparing the case with no crust at the wall. For example, the liquidus temperature of bulk melt, which is also the melt/crust interface temperature, decreased about 4 °C from test beginning to the steady state of 5kW period. This means that T_{mean} - $T_{\text{int, original}}$.

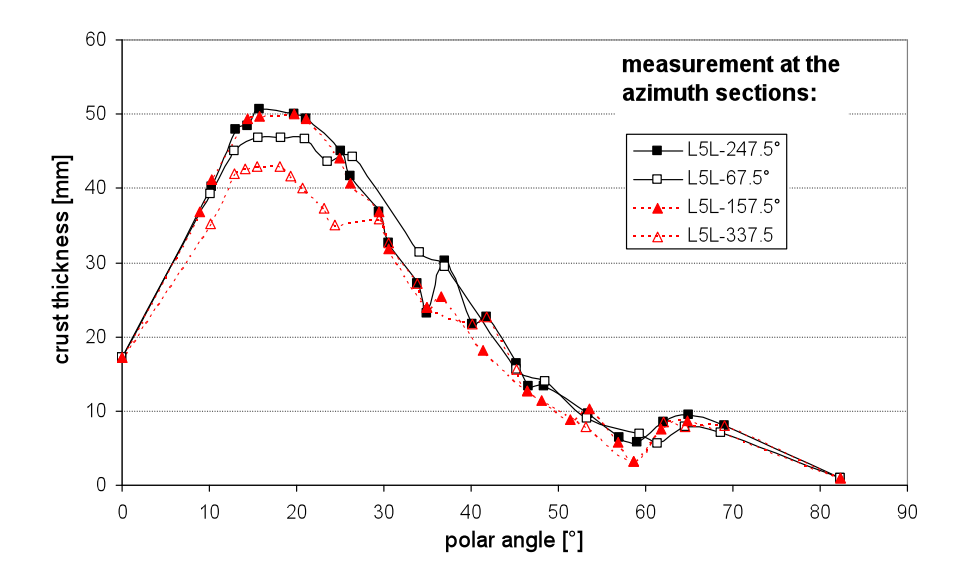


Figure 13 Crust thickness profile measured after L5L test at four azimuth sections

4. Conclusion

Both transient and steady state melt pool behaviour in RPV lower head were investigated in L4 and L5L tests, in which several times of melt pouring and power density transition were performed. The results demonstrated that melt pouring pattern and prompt change of power density have little influence on the homogeneity of horizontal melt temperature, but resulted in crust deformation such like gap formation or crust cracking which have different consequence on the crust thickness. The crust development can affect the melt/crust interface temperature, thus also the heat transfer through the vessel wall. At steady state, the dimensionless melt pool temperature and dimensionless heat flux weighted by their global mean value can be well characterized independent of power density, but they are dependent on melt pool height. Melt pool is consisted of a temperature-stratified lower region and a temperature-homogenous upper region. Comparing with a low pool, the temperature slop in the stratified lower layer in a high pool is smaller and the maximum dimensionless temperature difference in the upper layer is lower. Also the maximum dimensionless heat flux in a high pool is lower than in a low pool. Above results can give indication of the behaviour of a prototypical melt pool with homogenous composition: the focusing effect of melt temperature and heat flux toward the pool upper surface is more significant in a low melt pool than in a high pool, although the absolute melt temperature and the maximum heat flux are dependent on power density.

References

[1] F. Kretzschmar, B. Fluhrer "Behavior of the Melt Pool in the Lower Plenum of the Reactor Pressure Vessel, Review of Experimental Programs and Background of the LIVE Program", Scientific report FZKA 7382, pp. 5.

- [2] S. Abalin. I. Gnidoi. V. Semenov. V. Strizhov. A. Surenkov. "The Results and Analysis of the RASPLAV Salt Tests". <u>Rasplav Seminar 2000</u>. Munich. Germany. 14-15 November 2000.
- [3] M. Helle, O. Kymäläinen, H. Tuomisto, "Experimental COPO II data on natural convection in homogenous and stratified pools", <u>NURETH-9</u>, San Francisco, California, October 1999.
- [4] J.M. Bonnet, J. M. Seiler, "Thermal hydraulic phenomena in corium pools: the BALI experiment", <u>17th ICONE</u>, Tokyo, Japan, April 1999, Nr. 7057.
- [5] B.R. Sehgal, "Accomplishments and challenges of the severe accident research", Nuclear Engineering and Design 210 (2001), pp. 79-84.
- [6] V. Asmolov. N.N. Ponomarev-Stepnoy, V. Strizhov, B.R. Sehgal, "Challenges Left in the Area of In-Vessel Melt Retention", Nuclear Engineering and Design, 209 (2001), pp. 87-96.
- [7] A. Miassoedov, T. Cron, J. Foit, S. Schmidt-Stiefel, T. Wenz, I. Ivanov, P. Popov, "Results of the LIVE-L1 Experiment on Melt Behaviour in RPV Lower Head Performed within the LACOMERA project at the Forschungszentrum Karlsruhe", 2007, Proc. 15th International Conference on Nuclear Engineering (ICONE15), Nagoya, Japan, April 22-26, 2007, Paper 10227.
- [8] X. Gaus-Liu, A. Miassoedov, T. Cron, J. Foit, T. Wennz, S. Schmidt-Stiefel, "Core melt solidification characteristics in PRV Lower head-Experimental results from LLIVE tests", J. of Engineering for Gas Turbines and Power", vol 132, 102924, 2010.
- [9] X. Gaus-Liu, A. Miassoedov, . Cron and T. Wenz, "The coolibility of melt pool in PWR lower head-results of LIVE experiments", Journal of Energy and Power Engineering, Vol. 4, Number 3, March 2010, pp. 15
- [10] X. Gaus-Liu, A. Miassoedov, T. Cron, T. Wenz, "In-vessel melt pool coolibility test-description and results of LIVE experiments", Nuclear Engineering and Design 240(2010), pp. 3898.
- [11] A. Palagin, F. Kretzschmar, V. Chudanov, "LIVE test FSt4: experimental results and simulation by CONV code", <u>The 13th International Topical Meeting on Nuclear Reactor Thermal Hydraulics (NURETH-13)</u>, Kanazawa City, Japan, September 27-October 2, 2009.
- [12] M. Buck, M. Bürger, A. Miassoedov, X. Gaus-Liu, A. Palagin, L. Godin-Jacqmin, C.T. Tran, W.M.Ma, V. Chudanov, "The LIVE program: tests and joint interpretation within SARNET and ISTC", <u>The 3rd European Review Meeting on Severe Accident Research (ERMSAR-2008)</u>, Nesseber, Bulgaria, 23-25 September 2008.
- [13] M. Buck, M. Bürger, A. Miassoedov, X. Gaus-Liu, A. Palagin, L. Godin-Jacqmin, C.T. Tran, W.M. Ma, V. Chudanov, "The LIVE program Results of test L1 and joint analyses on transient molten pool thermal hydraulics", Progress in Nuclear Energy, 52 (2010), pp. 46–60.

- [14] X. Gaus-Liu, B. Fluhrer, A. Miassoedov, T. Cron, J. Foit, S. Schmidt-Stiefel, T. Wenz; Results of the LIVE-L3A Experiment, KIT Scientific reports 7542, ISBN 978-3-86644-505-5, pp. 40.
- [15] A. Miassoedov, T. Cron, J. Foit, X. Gaus-Liu. A. Palagin, S. Schmidt-Stiefel, T. Wenz, "Results of the LIVE-L4 experiment on the melt behaviour in the RPV lower head", ICONE18, Xi'an, China, May 2010, ICONE18-29601
- [16] E.M. Levin, C.R. Robbins, H.F. McMurdie, 1985, "Phase Diagrams For Ceramists Vol. 1: Oxides and Salts", American Ceramic Society, ISBN-10: 0916094049.
- [17] R.W. Berg et al., 2004, "The NaNO₃/KNO₃ system: the position of the solidus and subsolidus", Dalton Trans., pp. 2224-2229.
- [18] H.M. Goodwin, and R.D. Mailey, "On the Density, Electrical Conductivity and Viscosity of Fused Salts and Their Mixtures", The Physical Review American Physical Society, January, 1980, pp. 40.
- [19] Flemmings, "Solidification Processing", Materials Science and Engineering Series, ISBN 0-07-021283-x, pp.59-66.
- [20] B.R. Sehgal, Z.L. Yang, "Ex-vessel Core Melt Stabilization Research; On the Experments with Simulant Materials at KTH", <u>SAM-ECOSTAR-P11/001</u>, KTH, Stockholm, Sweden, January 2001.